Unmanned Systems, Vol. 11, No. 1 (2023) 67–82

DOI: 10.1142/S2301385023500024

UNMANNED SYSTEMS
https://www.worldscientific.com/worldscinet/us

A Dynamic Leader–Follower Approach for Line Marching of Swarm Robots

He Cai, Shuping Guo, Huanli Gao*

School of Automation Science and Engineering,
South China University of Technology, Guangzhou 510641, P. R. China

Most of the existing exact formation algorithms for swarm systems are fully label-specified, i.e. the desired position for each individual in the formation is predetermined by its label, which would inevitably make the formation algorithms vulnerable to individual failures. To address this issue, in this paper, we propose a dynamic leader–follower approach to solving the line marching problem for a swarm of planar kinematic robots. In contrast to the existing results, the desired positions for the robots in the line are no longer predetermined by the robots' labels, but the relativity of the robots' labels as well as their real-time relative positions. By constantly forming the leader–follower chain, exact line marching can be realized by pairwise leader–following tracking. Since the order of the leader–follower chain keeps updating, the proposed algorithm shows strong robustness against robot failures. Comprehensive numerical results are provided to evaluate the performance of the proposed formation algorithm.

Keywords: Dynamic leader–follower approach; exact formation; line marching; swarm robots.

1. Introduction

Though individuals in a swarm are always subject to limited sensing, computing, decision and execution capability, the swarm as a whole exhibits marvelous performance. For example, by working in groups, the ant colony can move food hundreds of times heavier than their weights, thereby improving the foraging efficiency of the population [1]. Another typical example is the formation flying of geese, which helps to reduce energy expenditure and thus increases migration distance [2]. Inspired by the biological behaviors of social animals, formation control has received extensive attention which gives rise to a significant amount of research results revealing the underlying mechanism of the biological behaviors. In addition, formation control is also appealing from the perspective of engineering applications such as cooperative searching, exploration, escorting and commercial performance [3–7].

Roughly speaking, there are two main classes of control approaches to solving the formation control problem. The first class is the virtual structure approach [8–16], which treats formation as a single entity, and the formation is realized by keeping the relative position between a virtual leader and each agent. Early works establishing the virtual structure approach can be found in [8, 9]. Since after, the virtual structure approach has been advanced in several directions, such as dealing with system nonlinearity [10], integration with learning-based approach [11], special types of formation, such as circular formation [12], and adaptation to unreliable communication network [13], just to name a few. Recently, in [14], based on linear matrix inequality technique and common Lyapunov–Krasovskii stability theory, sufficient conditions for solving the time-varying formation problem for general linear multi-agent systems under switching interaction topologies and time-varying delays were investigated. Moreover, the work of [15] considered fixed-time event-triggered control schemes for time-varying formation tracking problem of leader–follower multi-agent systems subject to both continuous and intermittent communication. In [16], a distributed observer-based formation tracking algorithm was proposed

Received 1 September 2021; Accepted 16 February 2022; Published 27 April 2022. This paper was recommended for publication in its revised form by editorial board member, Jinwen Hu.
Email Address: *hlgao@scut.edu.cn

for multiple targets encircling. A salient advantage of the virtual structure approach lies in that it makes it easy to define formation. However, the definition of formation is fully label-specified by the virtual structure approach, i.e., the desired position for each individual in the formation is predetermined by its label. Consequentially, once an individual fails, the formation will be incomplete unless some further re-organization is invoked. In this sense, the virtual structure approach is not robust enough, or flexible enough, in the face of individual failures.

The second class is the classic leader–follower approach [17–26], which decouples the formation control problem into a set of ordered leader–following tracking problem. By specifying a chain of leader–follower pair, formation can be defined by the relative position of each leader–follower pair. Seminal works for the leader–follower approach can be found in [17–19], which lay the foundation for various important extensions. For example, [20] considered input constraint. Reference [21] adopted a receding-horizon scheme in the expect of fast exponential convergence. Recently, in the absence of global position and direction measurement, [22] proposed a flexible formation approach to tracking multiple mobile robots based on estimated relative position. [23] proposed a hierarchical control structure for affine formation of a group of high-order multiagent system. By utilizing relative velocity and bearing measurements, a distributed control approach was synthesized by [24] which guaranteed a desired geometric pattern for the robots under persistent exciting condition. Chen and Dimarogonas [25] further considered the prescribed performance guarantees for the leader–follower formation control. Buckley and Egerstedt [26] revealed the possibilities on the types of formations for robots with bearing-only sensors based on the theory of infinitesimal shape-similarity. Due to the simple design philosophy, the classic leader–follower approach is easy to understand and implement in practice. While, since the order of the leader–follower chain must be predetermined, once an individual fails, the other individuals subsequential to the failed individual in the chain will pause, which makes the classic leader–follower approach vulnerable to individual failures.

In summary, it is difficult for both the virtual structure approach and the classic leader–follower approach to deal with individual failures. The reason behind this is these approaches are fully label-specified, which shall not adapt to uncertainties caused by robot faults and failures. To address this issue, in this paper, we further propose a novel leader–follower approach to solving the line marching problem for a swarm of planar kinematic robots. In contrast to the classic leader–follower approaches [17–26], the desired positions for the robots in the line are no longer predetermined by the robots' labels, but the relativity of the robots' labels as well as their real-time relative positions. By constantly forming a chain of leader–follower pairs, exact line marching can be realized by pairwise leader–following tracking. Since the order of the leader–follower chain keeps updating, the proposed approach is called the *dynamic* leader–follower approach to distinguish from the classic leader–follower approaches.

The main advantage of the dynamic leader–follower approach is it is inherently endowed strong robustness against robot failures. In particular, once a robot fails, the rest robots will immediately re-form a new leader–follower chain and march in a new line. The failed robot will be considered as an obstacle by other robots. If the failed robot could get back to normal, it will rejoin the swarm and the whole robot swarm will re-form, again, into a new line and keep marching forward.

The following notation is adopted in this paper. Let $\mathbb{R}$ and $\mathbb{N}$ denote the sets of real numbers and positive integers, respectively. Given $x \in \mathbb{N}$,

$$\underline{x} \triangleq \{y | y \in \mathbb{N}, y \leq x\}.$$

Given angle θ, the planar rotation matrix is defined as

$$\mathbf{R}(\theta) = \begin{pmatrix} \cos(\theta) & -\sin(\theta) \\ \sin(\theta) & \cos(\theta) \end{pmatrix}.$$

Given $x, y \in \mathbb{R}^2$, the inner product of x and y is denoted by $\langle x, y \rangle$. The boolean relation "or" is denoted by $\vee$. Given a nonzero vector $x \in \mathbb{R}^2$, let $\gamma(x) = x/||x||$ denote the unit vector which has the same direction as x does.

2. Task Description

In this paper, we consider a swarm of N planar kinematic robots moving in an unbounded region subject to M immobile or mobile obstacles. For convenience, it is assumed that the positions of all the robots and obstacles are expressed in a common coordinate system.

For $i \in \underline{N}$, the motion of the ith robot is described by the following equation:

$$\dot{p}_i(t) = v_i(t), \tag{1}$$

where $p_i(t), v_i(t) \in \mathbb{R}^2$ denote the position and velocity vector of the ith robot, respectively.

Let $\delta_i > 0$ denote the minimal safety distance for the ith robot.

For $i \in \underline{M}$, the motion of the ith obstacle is described by the following equation:

$$\dot{q}_i(t) = u_i(t), \tag{2}$$

where $q_i(t), u_i(t) \in \mathbb{R}^2$ denote the position and velocity vector of the ith obstacle, respectively. For immobile obstacles, $u_i(t) = 0$ for all $t \geq 0$.

January 5, 2023 2:15:45pm WSPC/284-US 2350002 ISSN: 2301-3850 2nd Reading

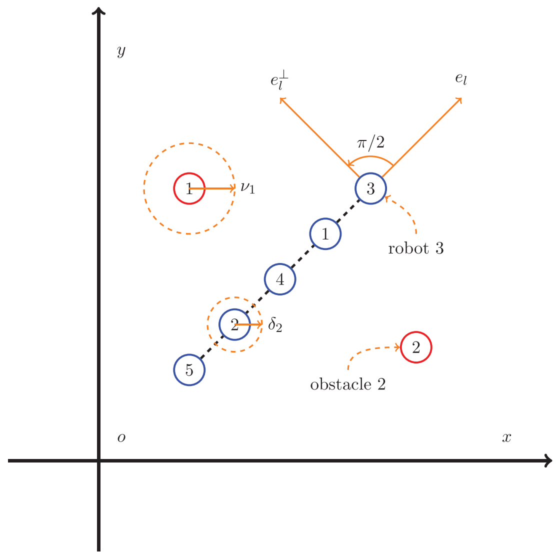

Fig. 1. An example of five robots marching in a line subject to two obstacles.

Let $\nu_i > 0$ denote the minimal safety distance for the ith obstacle.

Roughly speaking, as illustrated by Fig. 1, the task for the robots is to march in a line while keep collision avoidance for both obstacles and other robots. Let $v_l \in \mathbb{R}^2$ denote the nonzero marching velocity, and

$$e_l = \gamma(v_l) \tag{3}$$

denote the marching direction. Then, let

$$e_l^{\perp} = \mathbf{R}\left(\frac{\pi}{2}\right)e_l \tag{4}$$

denote the direction vector perpendicular to e_l by rotating e_l anticlockwise by 90°.

In what follows, for $i, j \in \underline{N}$, define

$$\begin{aligned} p_{i,j}(t) &= p_i(t) - p_j(t), \\ p_{i,j}^{l}(t) &= \langle p_{i,j}(t), e_l\rangle, \\ p_{i,j}^{\perp}(t) &= \langle p_{i,j}(t), e_l^{\perp}\rangle, \end{aligned} \tag{5}$$

and for $i \in \underline{N}$ and $j \in \underline{M}$,

$$\wp_{i,j}(t) = p_i(t) - q_j(t). \tag{6}$$

Mathematically, the line marching problem considered in this paper can be described as follows.

Problem 1. Design $v_i(t)$ of (1) such that the following two objectives can be simultaneously achieved:

- collision avoidance

(1) for all $t \geq 0$, for all $i, j \in \underline{N}$, $i \neq j$,

$$||p_{i,j}(t)|| \geq \delta_i + \delta_j. \tag{7}$$

(2) for all $t \geq 0$, for all $i \in \underline{N}$, $j \in \underline{M}$,

$$||\wp_{i,j}(t)|| \geq \delta_i + \nu_j. \tag{8}$$

- line marching

(1) for all $i \in \underline{N}$,

$$\lim_{t\to\infty}(v_i(t) - v_l) = 0. \tag{9}$$

(2) for all $i, j \in \underline{N}$,

$$\lim_{t\to\infty} p_{i,j}^{\perp}(t) = 0. \tag{10}$$

(3) there exists an order $(i_1, i_2, \ldots, i_N)$ with $i_k \in \underline{N}$ such that for $k \in \underline{N-1}$,

$$\lim_{t\to\infty} p_{i_k,i_{k+1}}^{l}(t) = \rho, \tag{11}$$

where $\rho > 0$ denotes the desired inter-robot distance.

To avoid the possible conflict between collision avoidance and line marching, ρ should be chosen such that

$$\rho \geq \max_{i,j\in\underline{N}, i\neq j}\{\kappa(\delta_i + \delta_j)\} \tag{12}$$

for some $\kappa > 1$.

Remark 1. Equation (11) indicates that the order of the marching line is immaterial as long as the relative position of the robots in the line can be maintained, which, in contrast to the classic leader–follower approaches, makes it possible that, when some robots fail, the rest robots can re-form a new marching line.

3. Line Marching Algorithm

To begin with, at time instant t, for robot i, we define the following indices:

(1) Head index:

$$\Lambda_i(t) = \begin{cases} 1 & \text{robot } i \text{ is the head of the line,} \\ 0 & \text{otherwise.} \end{cases}$$

(2) Leader index:

$$\Phi_i(t) = \begin{cases} 1 & \text{robot } i \text{ has a leader,} \\ 0 & \text{otherwise.} \end{cases}$$

(3) Follower index:

$$\Delta_i(t) = \begin{cases} 1 & \text{robot } i \text{ has a follower,} \\ 0 & \text{otherwise.} \end{cases}$$

(4) Failure index:

$$\Gamma_i(t) = \begin{cases} 0 & \text{robot } i \text{ fails,} \\ 1 & \text{otherwise.} \end{cases}$$

January 5, 2023 2:15:47pm WSPC/284-US 2350002 ISSN: 2301-3850 2nd Reading

(5) Pause index:

$$\Upsilon_i(t) = \begin{cases} 0 & \text{robot } i \text{ pauses,} \\ 1 & \text{otherwise.} \end{cases}$$

In general, $v_i(t)$ of (1) is given by

$$v_i(t) = \Gamma_i(t)\Upsilon_i(t)(v_{i,lm}(t) + v_{i,ca}(t)), \tag{13}$$

where $v_{i,lm}(t), v_{i,ca}(t) \in \mathbb{R}^2$ aim at line marching and collision avoidance, respectively.

To avoid collision, for robot i, we let

$$\begin{aligned} \bar{v}_{i,ca}(t) = &\sum_{j=1, j\neq i}^{N} \gamma(p_{i,j}(t))\zeta(\|p_{i,j}(t)\|, \delta_i, \delta_j, \kappa_1, \kappa_2) \\ &+ \sum_{j=1}^{M} \gamma(\wp_{i,j}(t))\zeta(\|\wp_{i,j}(t)\|, \delta_i, \nu_j, \kappa_1, \kappa_2), \end{aligned} \tag{14}$$

where $\kappa_1 > 1$, $\kappa_2 > 0$, and

$$\zeta(x, a, b, \kappa_1, \kappa_2) = \begin{cases} \left(\dfrac{\kappa_2}{x - (a+b)} - \dfrac{\kappa_2}{(\kappa_1 - 1)(a+b)}\right), & a + b < x \leq \kappa_1(a+b), \\ 0, & x > \kappa_1(a+b). \end{cases} \tag{15}$$

Note that by (15), we have

$$\lim_{x \to a+b} |\zeta(x, a, b, \kappa_1, \kappa_2)| = +\infty. \tag{16}$$

Suppose $a + b = 5$. For different κ_1 and κ_2, the plots of $\zeta(x, a, b, \kappa_1, \kappa_2)$ are given by Fig. 2. To ensure the existence of a steady solution to the line marching problem, it is necessary to assume that $\kappa > \kappa_1$.

To rule out the case that the robot might get stuck at some place when $v_{i,lm}(t) + \bar{v}_{i,ca}(t) = 0$, we let

$$v_{i,ca}(t) = \mathbf{R}(\theta_i(t))\bar{v}_{i,ca}(t), \tag{17}$$

where

$$\theta_i(t) = a_i \cdot \frac{\pi}{180} \cdot \sin \omega_i t, \tag{18}$$

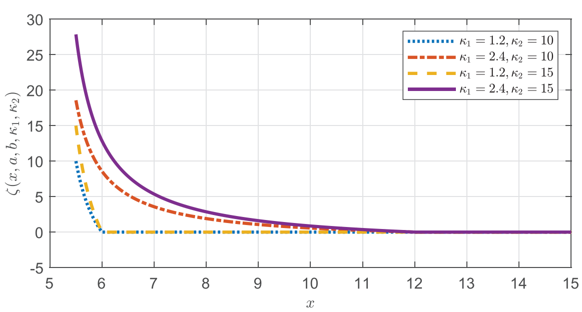

Fig. 2. The plots of $\zeta(x, a, b, \kappa_1, \kappa_2)$ for different κ_1 and κ_2 with $a + b = 5$.

where $0 < a_i < 90$, $\omega_i > 0$ are design parameters. By choosing a_i sufficiently small, the orientation of $\bar{v}_{i,ca}(t)$ shall constantly swing at a small amplitude, which would almost surely avoid the case of $v_{i,lm}(t) + \bar{v}_{i,ca}(t) = 0$.

For $j \neq i$, we let

$$v_{i,lm}^{j}(t) = \alpha(p_{j,i}^{l}(t) - \rho)e_l + \beta p_{j,i}^{\perp}(t)e_l^{\perp}, \tag{19}$$

where $\alpha, \beta > 0$ are control gains.

Now, we are ready to present the following line marching algorithm.

Algorithm 1. Line Marching Algorithm
Input: $p_1(t), \ldots, p_N(t)$.
Output: $v_1(t), \ldots, v_N(t)$.
for $i : 1 \to N$ **do**
  set $\Lambda_i(t) = 1$, $\Phi_i(t) = 0$, $\Delta_i(t) = 0$, $\Upsilon_i(t) = 0$.
for $i : 1 \to N$ **do**
  if $\Gamma_i(t) = 1$ **then**
    for $j : 1 \to N$, $j \neq i$ & $\Phi_i(t) = 0$ **do**
      if $p_{j,i}^{l}(t) > 0$ & $\Gamma_j(t) = 1$ **then**
        set $\Lambda_i(t) = 0$.
        if $\Delta_j(t) = 0$ **then**
          set $\Delta_j(t) = 1$, $\Phi_i(t) = 1$, $\Upsilon_i(t) = 1$.
          set $v_{i,lm}(t) = v_l + v_{i,lm}^{j}(t)$
    if $\Lambda_i(t) = 1$ **then**
      if $i = 1$ or $\Lambda_1(t) \vee \cdots \vee \Lambda_{i-1}(t) = 0$ **then**
        set $\Upsilon_i(t) = 1$.
        set $v_{i,lm}(t) = v_l$.
return result

Remark 2. The formation mechanism of the order of the leader–follower pairs under Algorithm 1 is explained as follows. Initially, all the robots consider themselves as the head of the line and pause by default. After indices initialization, the decision phase starts. Robot i checks the relative position between itself and other robots in the ascending order of the robot label. If there is at least one robot ahead of it along the marching direction, then robot i changes the status of its head index. Moreover, if robot i further finds a robot, say, robot j, ahead of it along the marching direction, which, in the meantime, has not been tailed, then robot j will be taken as the leader for robot i, and the decision loop of robot i ends. If a robot is the foremost one of the line, it automatically becomes the head of the line. If there are multiple robots situate as the foremost heads of the swarm, only the one with the smallest label will be selected as the leader of the line and others will pause. If a robot fails, it will stay where it is until it gets back to normal.

In what follows, we will present the stability analysis for Algorithm 1 under the following two assumptions.

Assumption 1. For all $t \geq 0$ and all $i \in \underline{N}$, $\Gamma_i(t) = 1$.

Assumption 2. $\underline{M} = 0$.

Theorem 1. *Under Assumptions* 1 *and* 2, *Problem* 1 *is solvable by Algorithm* 1.

Proof. Under Assumption 1, (13) reduces to

$$v_i(t) = \Upsilon_i(t)(v_{i,lm}(t) + v_{i,ca}(t)) \tag{20}$$

and under Assumption 2, (14) reduces to

$$\bar{v}_{i,ca}(t) = \sum_{j=1,j\neq i}^{N} \gamma(p_{i,j}(t))\zeta(||p_{i,j}(t)||, \delta_i, \delta_j, \kappa_1, \kappa_2). \tag{21}$$

We first show that collision will not happen. The inter-robot force can be classified into the combination of the attraction force, solely provided by $v^j_{i,lm}(t)$, and the repulsion force, possibly provided by $v^j_{i,lm}(t)$ and/or $v_{i,ca}(t)$.

Define

$$\ell(t) = \max_{i,j=1\ldots,N} ||p_{i,j}(t)||. \tag{22}$$

By keeping in mind that

$$\rho \geq \max_{i,j\in\underline{N},i\neq j}\{\kappa(\delta_i+\delta_j)\} > \max_{i,j\in\underline{N},i\neq j}\{\kappa_1(\delta_i+\delta_j)\} \tag{23}$$

for all $t \geq 0$, by (17) and (19), it follows that

$$\dot{\ell}(t) < 0 \text{ whenever } \ell(t) > \ell(0) + (N-2)\rho.$$

As a result, $\ell(t)$ will be globally bounded.

Consequentially, there exists $\varrho > 0$ such that for all $t \geq 0$ and all $i \in \underline{N}$,

$$||v_{i,lm}(t)|| \leq \varrho. \tag{24}$$

For $i \neq j$, let

$$V_{ij}(t) = \frac{1}{2} p_{i,j}(t)^T p_{i,j}(t). \tag{25}$$

Then,

$$\dot{V}_{ij}(t) = p_{i,j}(t)^T \dot{p}_{i,j}(t) = p_{i,j}(t)^T (v_i(t) - v_j(t)). \tag{26}$$

By Algorithm 1, without loss of generality, we consider the following three cases: (i) $\Upsilon_i(t) = 0$, $\Upsilon_j(t) = 0$; (ii) $\Upsilon_i(t) = 0$, $\Upsilon_j(t) = 1$; (iii) $\Upsilon_i(t) = 1$, $\Upsilon_j(t) = 1$.

For Case (i), $\dot{V}_{ij}(t) = 0$, which indicates no collision.

For Case (ii), it follows that

$$\begin{aligned}
\dot{V}_{ij}(t) &= -p_{i,j}(t)^T v_j(t) \\
&= -p_{i,j}(t)^T (v_{j,lm}(t) + v_{j,ca}(t)) \\
&= -p_{i,j}(t)^T v_{j,lm}(t) - p_{i,j}(t)^T [\mathbf{R}(\theta_j(t)) \\
&\quad \times \sum_{k=1,k\neq j}^{N} \gamma(p_{j,k}(t))\zeta(||p_{j,k}(t)||, \delta_j, \delta_k, \kappa_1, \kappa_2)] \\
&= -p_{i,j}(t)^T v_{j,lm}(t) + p_{i,j}(t)^T \mathbf{R}(\theta_j(t)) \\
&\quad \times \gamma(p_{i,j}(t))\zeta(||p_{i,j}(t)||, \delta_j, \delta_i, \kappa_1, \kappa_2) \\
&\quad - p_{i,j}(t)^T \Bigg[\mathbf{R}(\theta_j(t)) \sum_{k=1,k\neq i,j}^{N} \gamma(p_{j,k}(t)) \\
&\quad \times \zeta(||p_{j,k}(t)||, \delta_j, \delta_k, \kappa_1, \kappa_2)\Bigg] \\
&\triangleq \psi^a_{ij}(t) + \psi^b_{ij}(t) + \psi^c_{ij}(t),
\end{aligned} \tag{27}$$

where

$$\begin{aligned}
\psi^a_{ij}(t) &= -p_{i,j}(t)^T v_{j,lm}(t) \\
\psi^b_{ij}(t) &= p_{i,j}(t)^T \mathbf{R}(\theta_j(t))\gamma(p_{i,j}(t)) \\
&\quad \times \zeta(||p_{i,j}(t)||, \delta_j, \delta_i, \kappa_1, \kappa_2) \\
\psi^c_{ij}(t) &= -p_{i,j}(t)^T \Bigg[\mathbf{R}(\theta_j(t)) \sum_{k=1,k\neq i,j}^{N} \gamma(p_{j,k}(t)) \\
&\quad \times \zeta(||p_{j,k}(t)||, \delta_j, \delta_k, \kappa_1, \kappa_2)\Bigg].
\end{aligned}$$

By (24), $\psi^a_{ij}(t)$ is globally bounded for all $t \geq 0$.

Since $0 < a_j < 90$, it holds that

$$p_{i,j}(t)^T \mathbf{R}(\theta_j(t))\gamma(p_{i,j}(t)) > 0 \tag{28}$$

and hence

$$\lim_{||p_{i,j}(t)||\to\delta_i+\delta_j} \psi^b_{ij}(t) = +\infty. \tag{29}$$

Now, when $||p_{i,j}(t)|| \to \delta_i + \delta_j$, the sign of $\dot{V}_{ij}(t)$ depends on $\psi^c_{ij}(t)$. If $\psi^c_{ij}(t)$ is bounded, then there exists $\epsilon_{ij} > 0$ such that

$$\dot{V}_{ij}(t) > 0 \text{ whenever } V_{ij}(t) \leq \epsilon_{ij} \tag{30}$$

and hence no collision will occur between robot *i* and robot *j*. Another possibility is that $\psi^c_{ij}(t) \to -\infty$ so that the sign of $\dot{V}_{ij}(t)$ can still be negative when $||p_{i,j}(t)|| \to \delta_i + \delta_j$. Note that this can only happen when robots *i* and *j* are repelled by other robots, which further indicates that the robots repelling robots *i* and *j* must also be repelled by robots other than robots *i*, *j* and themselves. By repeating this process, it would need unlimited number of robots so that $\psi^c_{ij}(t) \to -\infty$, which obviously contradicts with the fact that the number of the robots is limited. Thus, overall, no collision will occur for Case (ii).

For Case (iii), it follows that

$$\begin{aligned}
\dot{V}_{ij}(t) &= p_{i,j}(t)^T (v_{i,lm}(t) + v_{i,ca}(t) - v_{j,lm}(t) - v_{j,ca}(t)) \\
&= p_{i,j}(t)^T (v_{i,lm}(t) - v_{j,lm}(t)) + p_{i,j}(t)^T \\
&\quad \times \Bigg[\mathbf{R}(\theta_i(t)) \sum_{k=1,k\neq i}^{N} \gamma(p_{i,k}(t))\zeta(||p_{i,k}(t)||, \delta_i, \delta_k, \kappa_1, \kappa_2)
\end{aligned}$$

$$
\begin{aligned}
&-\mathbf{R}(\theta_j(t))\sum_{k=1,k\neq j}^{N}\gamma(p_{j,k}(t))\\
&\times\zeta(\|p_{j,k}(t)\|,\delta_j,\delta_k,\kappa_1,\kappa_2)\Bigg]\\
&= p_{i,j}(t)^T(v_{i,lm}(t)-v_{j,lm}(t))+p_{i,j}(t)^T\mathbf{R}(\theta_i(t))\\
&\quad\times\gamma(p_{i,j}(t))\zeta(\|p_{i,j}(t)\|,\delta_i,\delta_j,\kappa_1,\kappa_2)\\
&\quad+p_{i,j}(t)^T[\mathbf{R}(\theta_i(t))\sum_{k=1,k\neq i,j}^{N}\gamma(p_{i,k}(t))\\
&\quad\times\zeta(\|p_{i,k}(t)\|,\delta_i,\delta_k,\kappa_1,\kappa_2)]+p_{i,j}(t)^T\mathbf{R}(\theta_j(t))\\
&\quad\times\gamma(p_{i,j}(t))\zeta(\|p_{i,j}(t)\|,\delta_i,\delta_j,\kappa_1,\kappa_2)\\
&\quad-p_{i,j}(t)^T\Bigg[\mathbf{R}(\theta_j(t))\sum_{k=1,k\neq i,j}^{N}\gamma(p_{j,k}(t))\\
&\quad\times\zeta(\|p_{j,k}(t)\|,\delta_j,\delta_k,\kappa_1,\kappa_2)\Bigg]\\
&=\psi_{ij}^a(t)+\psi_{ij}^b(t)+\psi_{ij}^c(t),
\end{aligned}\tag{31}
$$

where

$$
\begin{aligned}
\psi_{ij}^a(t) &= p_{i,j}(t)^T(v_{i,lm}(t)-v_{j,lm}(t)),\\
\psi_{ij}^b(t) &= p_{i,j}(t)^T[\mathbf{R}(\theta_i(t))+\mathbf{R}(\theta_j(t))]\gamma(p_{i,j}(t))\\
&\quad\times\zeta(\|p_{i,j}(t)\|,\delta_i,\delta_j,\kappa_1,\kappa_2),\\
\psi_{ij}^c(t) &= p_{i,j}(t)^T\Bigg[\mathbf{R}(\theta_i(t))\sum_{k=1,k\neq i,j}^{N}\gamma(p_{i,k}(t))\\
&\quad\times\zeta(\|p_{i,k}(t)\|,\delta_j,\delta_k,\kappa_1,\kappa_2)\Bigg]\\
&\quad-p_{i,j}(t)^T\Bigg[\mathbf{R}(\theta_j(t))\sum_{k=1,k\neq i,j}^{N}\gamma(p_{j,k}(t))\\
&\quad\times\zeta(\|p_{j,k}(t)\|,\delta_j,\delta_k,\kappa_1,\kappa_2)\Bigg].
\end{aligned}
$$

Similar to Case (ii), $\psi_{ij}^a(t)$ is globally bounded for all $t\geq 0$.

Since $0<a_i,a_j<90$, it holds that

$$p_{i,j}(t)^T[\mathbf{R}(\theta_i(t))+\mathbf{R}(\theta_j(t))]\gamma(p_{i,j}(t))>0. \tag{32}$$

Therefore,

$$\lim_{\|p_{i,j}(t)\|\to\delta_i+\delta_j}\psi_{ij}^b(t)=+\infty. \tag{33}$$

The rest proof can be obtained by contradiction similar to the analysis of Case (ii) and thus is omitted.

Now, we are able to conclude that collision avoidance can be achieved.

Next, we will show that line marching can be achieved asymptotically. At $t=0$, there will be a unique robot, labeled as i_1, such that $\Lambda_{i_1}(0)=1$ and $\Upsilon_{i_1}(0)=1$. Let

$$\bar{v}(t)=\frac{1}{N}\sum_{i=1}^{N}v_i(t). \tag{34}$$

Then by (20), there exists $T_1\geq 0$ such that for all $t\geq T_1$,

$$\langle\bar{v}(t),e_l\rangle>0. \tag{35}$$

As a result, there exists $T_2\geq 0$ such that for all $t\geq T_2$ and all $i\in\underline{N}$, $\Upsilon_i(t)=1$. It is worth mentioning that the priorities for leader selection of the robots under Assumption 1 are different. In particular, the robots with small labels have the priorities in selecting leaders. Consequentially, there will be no stable oscillation in the formation process of the order of the leader–follower pairs. Moreover, in the presence of $\mathbf{R}(\theta_i(t))$, robots will not get stuck due to the balance of attraction force and the repulsion force. As a result, by Algorithm 1, there exists $T_3\geq 0$ such that for all $t\geq T_3$, the robots other than i_1 can be labeled as $i_2,\ldots,i_N$ in the following way:

$$p_{i_1,i_2}^l(t)<p_{i_1,i_3}^l(t)<\cdots<p_{i_1,i_N}^l(t). \tag{36}$$

On the other hand, for $t\geq T_3$,

$$\langle v_{i_1,ca}(t),e_l\rangle\geq 0 \tag{37}$$

and

$$\langle v_{i_N,ca}(t),e_l\rangle\leq 0. \tag{38}$$

Therefore, there exists $T_4\geq 0$ such that for all $t\geq T_4$ and all $k\in\underline{N-1}$,

$$p_{i_k,i_{k+1}}^l(t)>\kappa_1(\delta_{i_k}+\delta_{i_{k+1}}). \tag{39}$$

That is, the inter-robot repulsion force induced by (17) will vanish in finite time. Let $T=\max\{T_1,T_2,T_3,T_4\}$. Thus, for all $t\geq T$,

$$
\begin{aligned}
\dot{p}_{i_1,i_2}(t) &= v_l-v_l-\alpha(p_{i_1,i_2}^l(t)-\rho)e_l-\beta p_{i_1,i_2}^{\perp}(t)e_l^{\perp}\\
&= -\alpha(p_{i_1,i_2}^l(t)-\rho)e_l-\beta p_{i_1,i_2}^{\perp}(t)e_l^{\perp}.
\end{aligned}\tag{40}
$$

Then, noting that $\langle e_l,e_l\rangle=1$ and $\langle e_l,e_l^{\perp}\rangle=0$ gives

$$\dot{p}_{i_1,i_2}^l(t)=-\alpha(p_{i_1,i_2}^l(t)-\rho) \tag{41}$$

and

$$\dot{p}_{i_1,i_2}^{\perp}(t)=-\beta p_{i_1,i_2}^{\perp}(t). \tag{42}$$

As a result,

$$\lim_{t\to\infty}p_{i_1,i_2}^l(t)=\rho,\ p_{i_1,i_2}^{\perp}(t)=0. \tag{43}$$

Next, suppose for all $t\geq T$,

$$\lim_{t\to\infty}p_{i_k,i_{k+1}}^l(t)=\rho,\quad \lim_{t\to\infty}p_{i_k,i_{k+1}}^{\perp}(t)=0. \tag{44}$$

Then, for all $t \geq T$, we have

$$\begin{aligned}\dot{p}_{i_{k+1},i_{k+2}}(t) &= v_l + \alpha(p^l_{i_k,i_{k+1}}(t) - \rho)e_l + \beta p^\perp_{i_k,i_{k+1}}(t)e_l^\perp \\ &\quad - v_l - \alpha(p^l_{i_{k+1},i_{k+2}}(t) - \rho)e_l - \beta p^\perp_{i_{k+1},i_{k+2}}(t)e_l^\perp \\ &= \varsigma_{i_k,i_{k+1}}(t) - \alpha(p^l_{i_{k+1},i_{k+2}}(t) - \rho)e_l - \beta p^\perp_{i_{k+1},i_{k+2}}(t)e_l^\perp,\end{aligned} \tag{45}$$

where

$$\varsigma_{i_k,i_{k+1}}(t) = \alpha(p^l_{i_k,i_{k+1}}(t) - \rho)e_l + \beta p^\perp_{i_k,i_{k+1}}(t)e_l^\perp. \tag{46}$$

Note that by (44),

$$\lim_{t\to\infty} \varsigma_{i_k,i_{k+1}}(t) = 0. \tag{47}$$

Moreover, we have

$$\dot{p}^l_{i_{k+1},i_{k+2}}(t) = -\alpha(p^l_{i_{k+1},i_{k+2}}(t) - \rho) + \langle \varsigma_{i_k,i_{k+1}}(t), e_l \rangle \tag{48}$$

and

$$\dot{p}^\perp_{i_{k+1},i_{k+2}}(t) = -\beta p^\perp_{i_{k+1},i_{k+2}}(t) + \langle \varsigma_{i_k,i_{k+1}}(t), e_l^\perp \rangle. \tag{49}$$

Thus by (47),

$$\lim_{t\to\infty} p^l_{i_{k+1},i_{k+2}}(t) = \rho, \quad \lim_{t\to\infty} p^\perp_{i_{k+1},i_{k+2}}(t) = 0. \tag{50}$$

Then, by the induction method, for all $k \in \underline{N-1}$,

$$\lim_{t\to\infty} p^l_{i_k,i_{k+1}}(t) = \rho \tag{51}$$

and for all $i, j \in \underline{N}$,

$$\lim_{t\to\infty} p^\perp_{i,j}(t) = 0. \tag{52}$$

At the same time, for all $i \in \underline{N}$, $\Upsilon_i(t) = 1$, $v_{i,ca}(t) = 0$, $\lim_{t\to\infty} v^j_{i,lm}(t) = 0$. Thus,

$$\lim_{t\to\infty} (v_i(t) - v_l) = 0 \tag{53}$$

and hence the proof is complete. □

Remark 3. Without Assumption 1 or 2, theoretically, one can find counter examples that Algorithm 1 cannot solve Problem 1. For example, without Assumption 2, one cannot rule out the possibility that there are k obstacles forming a ring-like pattern which happens to enclose some of the robots, as shown by Fig. 3. In this case, the enclosed robots can no longer come out of the ring-like pattern due to the collision avoidance mechanism. The same outcome also applies to the case if we replace the obstacles with the malfunctioned robots if Assumption 1 is not valid. In this sense, no matter what algorithm is applied, Assumptions 1 and 2, or other assumptions with the same purpose as Assumptions 1 and 2, are necessary for Theorem 1. Nevertheless, these counter examples are, of course, very extreme cases with little chance to occur in practice.

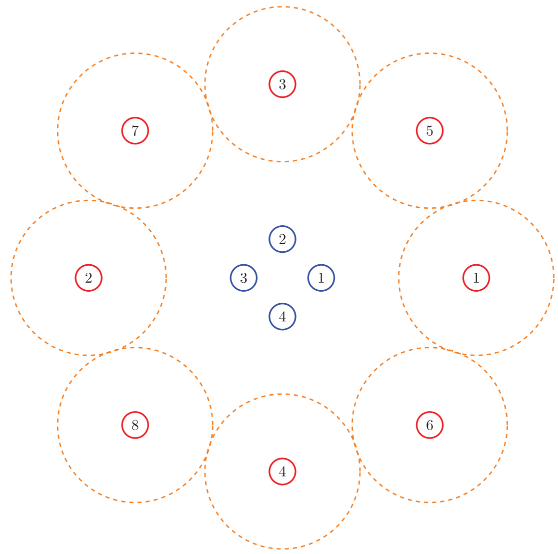

Fig. 3. A counter example without Assumption 2.

Therefore, as shown by the simulation studies in Sec. 4, Problem 1 can still be solved by Algorithm 1 without Assumption 1 or 2.

4. Numerical Simulations

In this section, we consider a swarm of 10 planar kinematic robots. The reference marching line is characterized by $v_l = (-8, 12)^T \triangleq (v_{lx}, v_{ly})^T$, $\rho = 4$. For simplicity, the minimal inter-robot safety distance is set to be $\delta_i \triangleq \delta = 1$. The control parameters are selected to be $\kappa_1 = 1.5$, $\kappa_2 = 10$, $a_i = 10$, $\omega_i = 1$, $\alpha = 10$, $\beta = 10$. Note that by the above setting, $\kappa = 2 > 1.5 = \kappa_1$. In the following, we will consider two cases for numerical simulation.

4.1. *The normal case*

First, we consider the normal case of line marching without robot failures subject to a mobile obstacle with $\nu_1 = 10$ and $u_1(t) = (15, 0)^T$. The initial positions of the robots are given by $p_1(0) = (-5, 10)^T$, $p_2(0) = (1, 20)^T$, $p_3(0) = (-10, 5)^T$, $p_4(0) = (5, 10)^T$, $p_5(0) = (10, 5)^T$, $p_6(0) = (0, 10)^T$, $p_7(0) = (5, -10)^T$, $p_8(0) = (15, -5)^T$, $p_9(0) = (-5, -10)^T$, $p_{10}(0) = (-10, -5)^T$. The initial position for the obstacle is given by $q_1(0) = (-90, 60)^T$.

Figure 4 shows the robots' and mobile obstacle's positions at different time instants. Figures 5(a) and 5(b) show the time profiles of robots' positions and velocities, respectively. It can be seen that the line marching objective has been successfully achieved. Figure 5(c) shows the relative distance between each robot and the mobile obstacle,

January 5, 2023 2:16:12pm WSPC/284-US 2350002 ISSN: 2301-3850

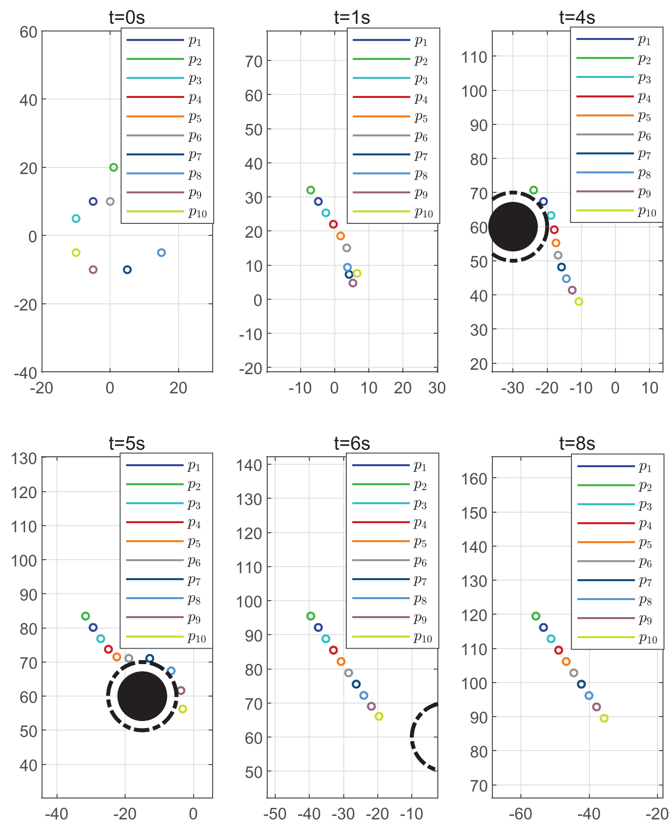

Fig. 4. Robots' and mobile obstacle's positions in Case 4.1.

and the minimal relative distance between two robots. It can be seen that all the lines are above the associated safety limits, indicating that there is no collision during the whole process.

4.2. *The case of robot failure: Comparisons with the virtual structure approach and the classic leader–follower approach*

In this case, we consider the scenario when a robot fails and show the comparisons between the virtual structure approach, the classic leader–follower approach, and the dynamic leader–follower approach proposed in this paper. For simplicity, initially, we assume the robots are already in line formation. In particular, we let $p_1(0) = (-12, 40)^T$, $p_2(0) = (-15, 44)^T$, $p_3(0) = (-10, 37)^T$, $p_4(0) = (-8, 34)^T$, $p_5(0) = (-6, 30)^T$, $p_6(0) = (-4, 27)^T$, $p_7(0) = (-1.5, 24)^T$, $p_8(0) = (0.5, 20.5)^T$, $p_9(0) = (2.5, -17)^T$, $p_{10}(0) = (5, 14)^T$. Suppose at $t = 1$ s, robot 4 fails.

The system performance using the virtual structure approach is shown by Fig. 6(a). Since the desired position by the virtual structure approach is predetermined by the labels of the robots, when robot 4 fails, there will be a vacancy in the formation which cannot be made up by other robots unless some further reconfiguration is invoked.

The system performance using the classic leader–follower approach is shown by Fig. 6(b). The order of the chain

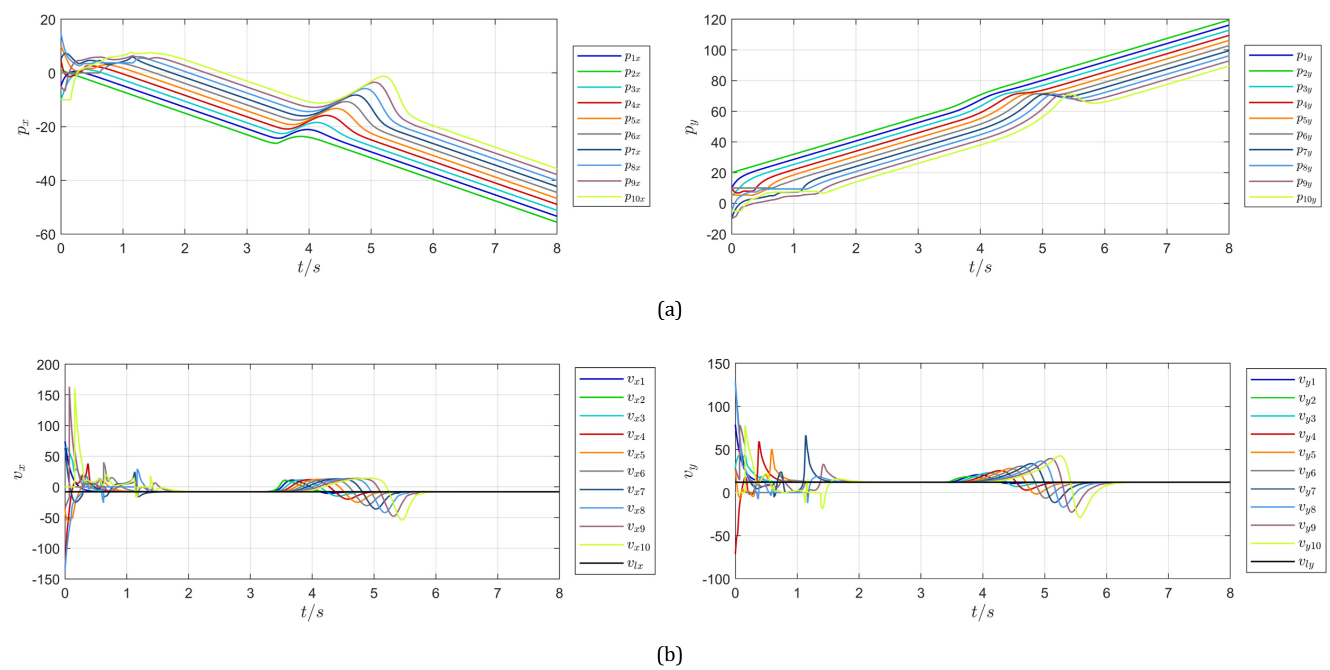

Fig. 5. Simulation results of Case 4.1: (a) time profiles of robots' positions; (b) time profiles of robots' velocities; (c) time profiles of the relative distance between each robot and the mobile obstacle, and the minimal relative distance between two robots.

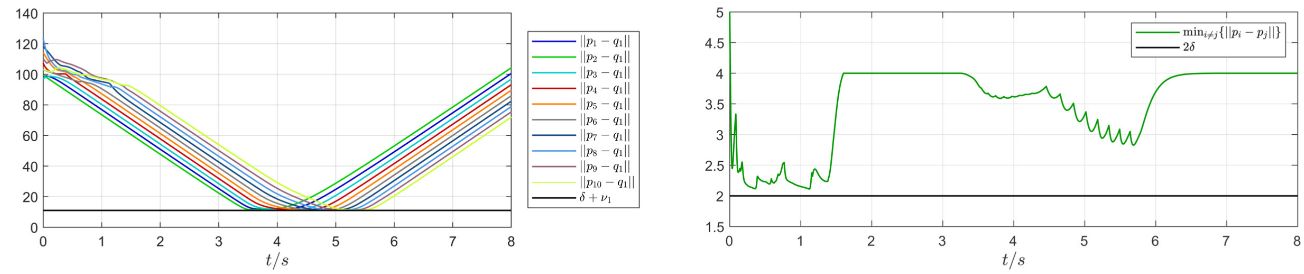

(c)

Fig. 5. (*Continued*)

of leader–follower pairs is set to be $(1, 2)$, $(2, 3)$, $(3, 4)$, $(4, 5)$, $(5, 6)$, $(6, 7)$, $(7, 8)$, $(8, 9)$, $(9, 10)$. It can be seen from the simulation results that, when robot 4 fails, robots 5–10 all get stuck since the order of the chain of leader–follower pairs shall not adapt to changes.

The system performance using the dynamic leader–follower approach proposed in this paper is shown by

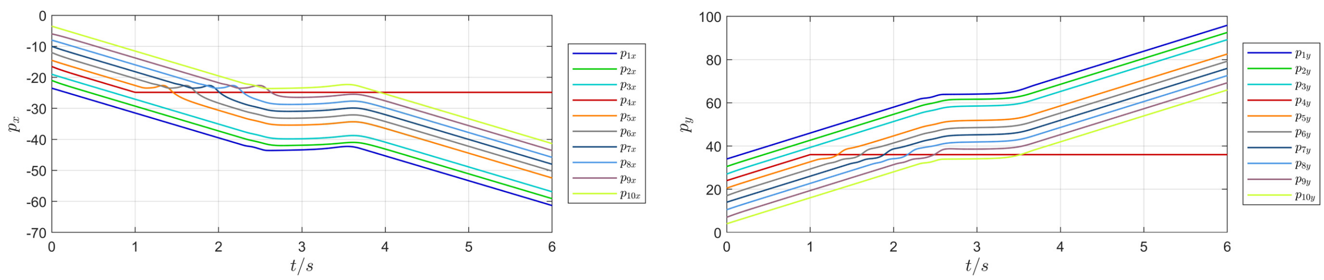

(a)

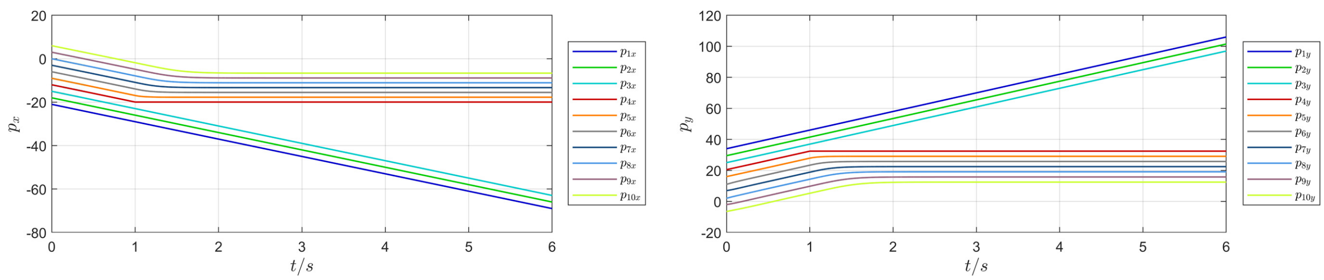

(b)

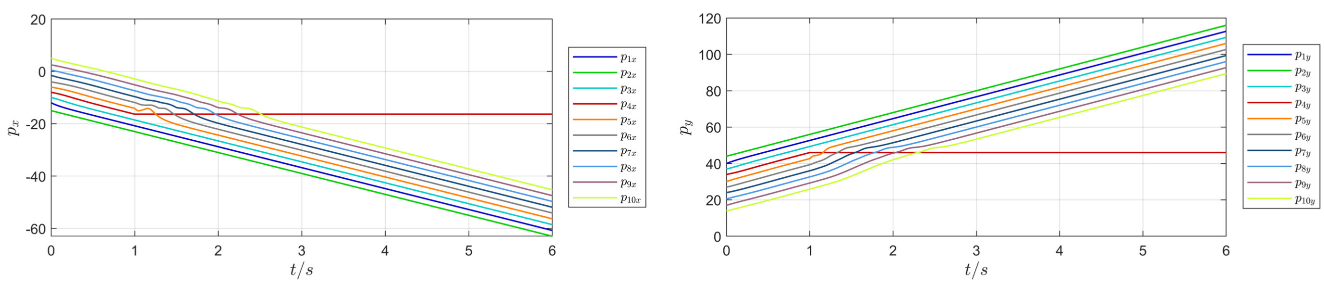

(c)

Fig. 6. Simulation results of Case 4.2 where robot 4 fails at $t = 1$s: (a) time profiles of robots' positions using the virtual structure approach; (b) time profiles of robots' positions using the classic leader–follower approach; (c) time profiles of robots' positions using the dynamic leader–follower approach.

Fig. 6(c). It can be seen from the simulation results that, when robot 4 fails, the rest robots has re-formed a new chain of leader–follower pairs, bypassed robot 4, and formed a new marching line, which shows strong robustness against robot failures.

5. Discrete-Time Model

In this section, we apply the proposed line marching algorithm to discrete-time model, where (1) and (2) become

$$p_i(k+1) = p_i(k) + Tv_i(k)$$

and

$$q_i(k+1) = q_i(k) + Tu_i(k),$$

respectively, where $T > 0$ denotes the sampling time. Note that the discretization of $v_{i,ca}(t)$ and $v^j_{i,lm}(t)$ by (17) and (19) are straightforward and thus are omitted. The line marching algorithm for the discrete-time case is given by Algorithm 2.

In this section, we also consider a swarm of 10 planar kinematic robots. The reference marching line are characterized by $v_l = (-8, 12)^T$, $\rho = 4$. The sampling time is chosen to be $T = 0.001$. The minimal inter-robot safety distance is set to be $\delta_i \triangleq \delta = 1$. The control parameters are selected to be $\kappa_1 = 1.5$, $\kappa_2 = 10$, $a_i = 10$, $\omega_i = 1$, $\alpha = 10$, $\beta = 10$. Still, $\kappa = 2 > 1.5 = \kappa_1$.

We consider the line formation subject to a mobile obstacle with $\nu_1 = 10$ and $u_1(t) = (15, 0)^T$. The initial positions of the robots are given by $p_1(0) = (-5, 10)^T$, $p_2(0) = (1, 20)^T$, $p_3(0) = (-10, 5)^T$, $p_4(0) = (5, 10)^T$, $p_5(0) = (10, 5)^T$, $p_6(0) = (0, 10)^T$, $p_7(0) = (5, -10)^T$, $p_8(0) = (15, -5)^T$, $p_9(0) = (-5, -10)^T$, $p_{10}(0) = (-10, -5)^T$. The initial position for the obstacle is given by $q_1(0) = (-80, 60)^T$.

Algorithm 2. Line Marching Algorithm
Input: $p_1(k), \dots, p_N(k)$.
Output: $v_1(k), \dots, v_N(k)$.
for $i = 1 \to N$ **do**
  set $\Lambda_i(k) = 1$, $\Phi_i(k) = 0$, $\Delta_i(k) = 0$, $\Upsilon_i(k) = 0$.
for $i = 1 \to N$ **do**
  if $\Gamma_i(k) = 1$ **then**
    for $j = 1 \to N$, $j \neq i$, & $\Phi_i(k) = 0$ **do**
      if $p^l_{j,i}(k) > 0$ & $\Gamma_j(k) = 1$ **then**
        set $\Lambda_i(k) = 0$.
        if $\Delta_j(k) = 0$ **then**
          set $\Delta_j(k) = 1$, $\Phi_i(k) = 1$, $\Upsilon_i(k) = 1$.
          set $v_{i,lm}(k) = v_l + v^j_{i,lm}(k)$.
    if $\Lambda_i(k) = 1$ **then**
      if $i = 1$ or $\Lambda_1(k) \vee \cdots \vee \Lambda_{i-1}(k) = 0$ **then**
        set $\Upsilon_i(k) = 1$.
        set $v_{i,lm}(k) = v_l$.
return result

Suppose the simulation process consists of four phases:

(1) $k \in [0, 3000]$, the robots will asymptotically form into a line from the initial positions;
(2) $k \in [3000, 8000]$, the robots will bypass the mobile obstacle and re-form a marching line;
(3) $k \in [8000, 11, 000]$, robot 4 fails;
(4) $k \in [11, 000, 15, 000]$, robot 4 gets back to normal and rejoins the robot swarm.

Figure 7 shows the robots' and mobile obstacle's positions during the whole simulation process. It can be seen that the robot swarm has first managed to form a marching line, and then successfully bypassed the mobile obstacle. When robot 4 fails, other robots consider robot 4 as an immobile obstacle and has re-formed a new marching line. After robot 4 gets back to normal, it rejoins the marching line, which happens to be at the same position before the event of failure.

Figures 8(a) and 8(b) show the time profiles of the robots' positions and velocities, respectively. It can be seen that the line marching objective has been successfully achieved. Figure 8(c) shows the relative distance between each robot and the mobile obstacle, and the minimal relative distance between two robots, which indicates no collision as expected.

6. Unicycle Model

In this section, we consider a more practical situation where the robot is described by the unicycle model, and the numerical simulation is performed on the ROS platform. In particular, for $i \in \underline{N}$, the kinematic equations of the ith robot are given by

$$\begin{aligned} \dot{p}_i(t) &= \upsilon_i(t)\begin{pmatrix} \cos\vartheta_i(t) \\ \sin\vartheta_i(t) \end{pmatrix}, \\ \dot{\vartheta}_i(t) &= \varpi_i(t), \end{aligned} \tag{54}$$

where $p_i(t) \in \mathbb{R}^2$, $\vartheta_i(t) \in \mathbb{R}$ denote the position and heading angle of the ith robot, respectively, and $\upsilon_i(t) \in \mathbb{R}$, $\varpi_i(t) \in \mathbb{R}$ denote the linear and angular velocity, respectively.

Let l_i denote the distance between the wheel pair of the ith robot, and then

$$\begin{aligned} \upsilon_{il}(t) &= \upsilon_i(t) - \frac{1}{2} l_i \varpi_i(t), \\ \upsilon_{ir}(t) &= \upsilon_i(t) + \frac{1}{2} l_i \varpi_i(t), \end{aligned} \tag{55}$$

denote the speeds of left wheel and the right wheel of the robot, respectively. Since system (54) is nonlinear, the

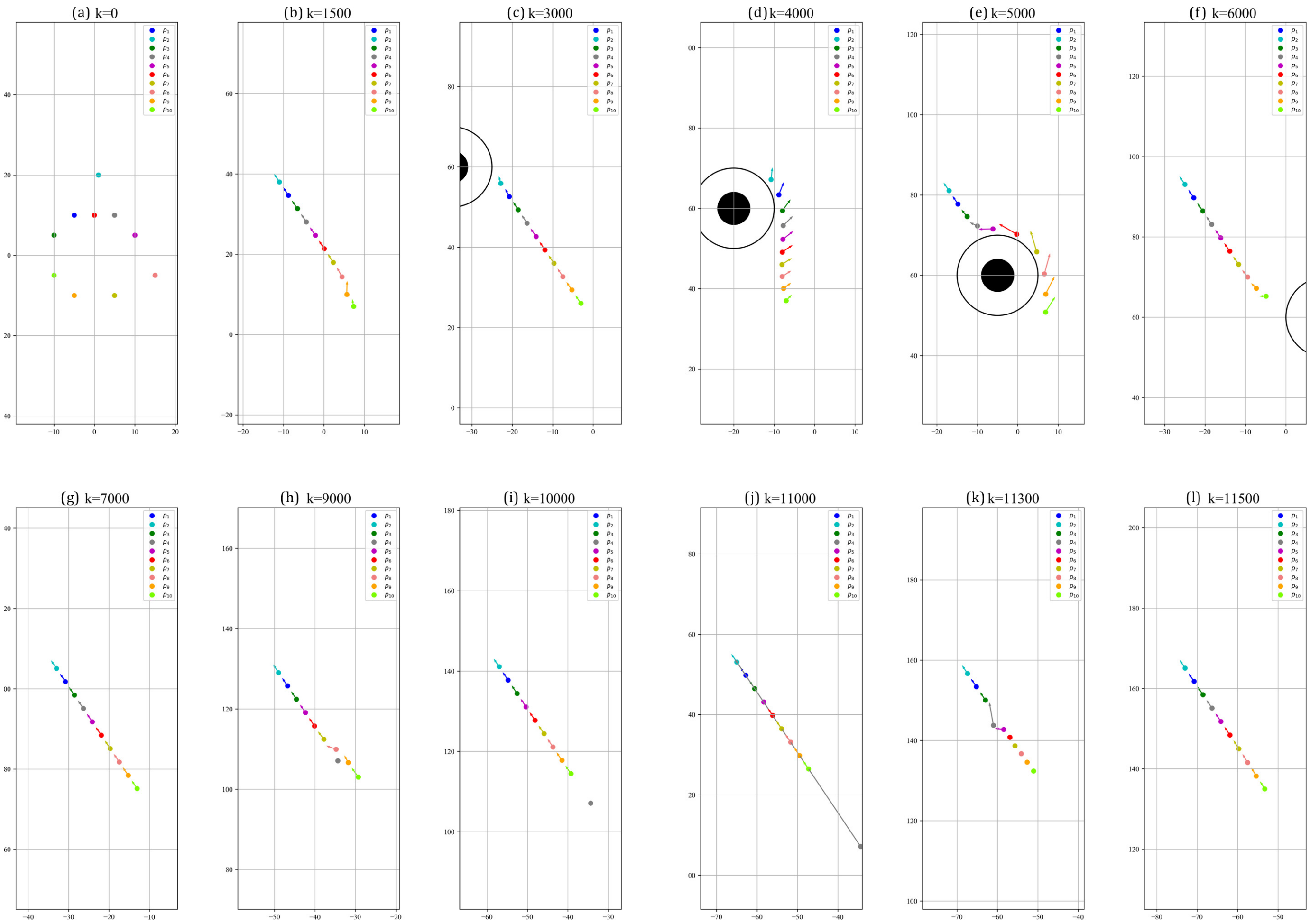

Fig. 7. Robots' and mobile obstacle's positions for the discrete-time case.

proposed line marching algorithm cannot be applied directly. To tackle this issue, we perform the following coordinate transformation as in [27]:

$$\bar{p}_i(t) = p_i(t) + d_i \begin{pmatrix} \cos\vartheta_i(t) \\ \sin\vartheta_i(t) \end{pmatrix}, \tag{56}$$

where $d_i > 0$ denotes some small offset to avoid singularity in coordinate transformation. Then it follows that

$$\dot{\bar{p}}_i(t) = \dot{p}_i(t) + d_i \varpi_i(t) \begin{pmatrix} -\sin\vartheta_i(t) \\ \cos\vartheta_i(t) \end{pmatrix}$$

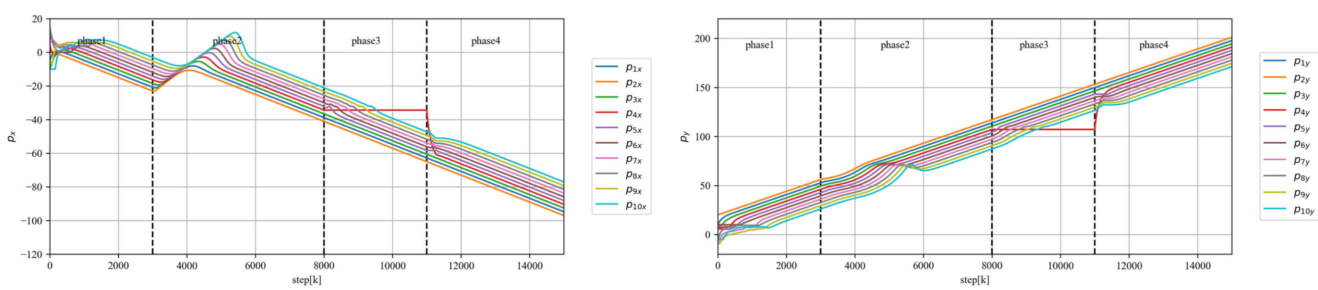

(a)

Fig. 8. Simulation results for the discrete-time case: (a) robots' positions; (b) robots' velocities; (c) relative distance between each robot and the mobile obstacle, and the minimal relative distance between two robots.

January 5, 2023 2:17:35pm WSPC/284-US 2350002 ISSN: 2301-3850 2nd Reading

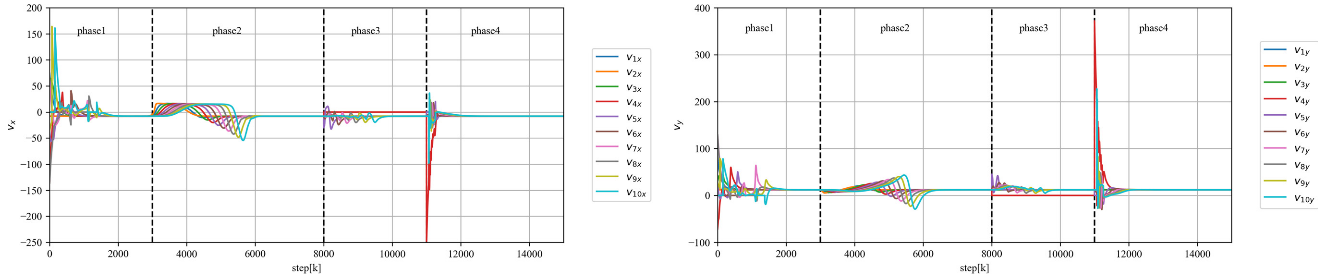

(b)

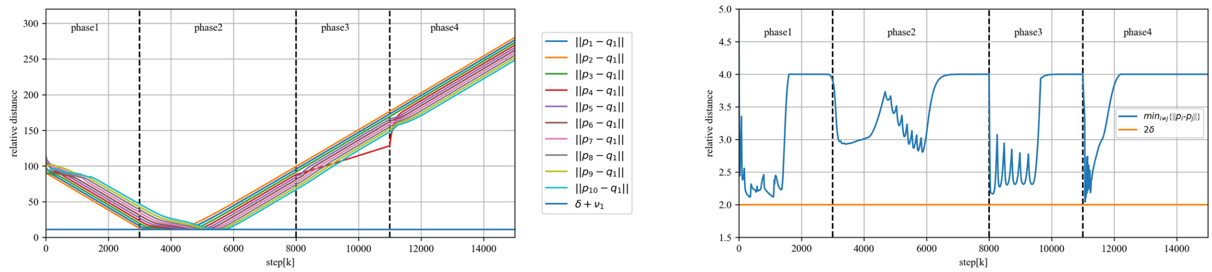

(c)

Fig. 8. (*Continued*)

$$= v_i(t)\begin{pmatrix} \cos\vartheta_i(t) \\ \sin\vartheta_i(t) \end{pmatrix} + d_i\varpi_i(t)\begin{pmatrix} -\sin\vartheta_i(t) \\ \cos\vartheta_i(t) \end{pmatrix}$$
$$= \begin{pmatrix} \cos\vartheta_i(t) & -d_i\sin\vartheta_i(t) \\ \sin\vartheta_i(t) & d_i\cos\vartheta_i(t) \end{pmatrix}\begin{pmatrix} v_i(t) \\ \varpi_i(t) \end{pmatrix}.$$

Let

$$\Theta_i(t) = \begin{pmatrix} \cos\vartheta_i(t) & -d_i\sin\vartheta_i(t) \\ \sin\vartheta_i(t) & d_i\cos\vartheta_i(t) \end{pmatrix}$$

and

$$\bar{v}_i(t) = \Theta_i(t)\begin{pmatrix} v_i(t) \\ \varpi_i(t) \end{pmatrix}.$$

Then, we have

$$\dot{\bar{p}}_i(t) = \bar{v}_i(t). \tag{57}$$

Moreover, it can be verified that for all $t \geq 0$, $\Theta_i(t)$ is non-singular whose inverse is given by

$$\Theta_i(t)^{-1} = \begin{pmatrix} \cos\vartheta_i(t) & \sin\vartheta_i(t) \\ -\sin\vartheta_i(t)/d_i & \cos\vartheta_i(t)/d_i \end{pmatrix}.$$

By using the coordinate transformation (56), the nonlinear system (54) is transformed into a linear kinematic system (57), which is in the same form of (1) and thus the proposed algorithm is applicable. After obtaining $\bar{v}_i(t)$, the linear and angular velocity inputs to system (54) are given by

$$\begin{pmatrix} v_i(t) \\ \varpi_i(t) \end{pmatrix} = \Theta_i(t)^{-1}\bar{v}_i(t) \tag{58}$$

and then the speeds of left and right wheel of the robot can be determined by Eq. (55).

Note that in ROS platform, the position measurements of the robots are subject to the Gaussian noise. As a result, the co-leader situation shall not occur. Thus, Algorithm 1 can be further simplified into Algorithm 3 as follows.

Algorithm 3. Line Marching Algorithm
Input: $p_1(t), \ldots, p_N(t)$.
Output: $v_1(t), \ldots, v_N(t)$.

for $i = 1 \to N$ **do**
  set $\Lambda_i(t) = 1$, $\Phi_i(t) = 0$, $\Delta_i(t) = 0$, $\Upsilon_i(t) = 0$.
for $i = 1 \to N$ **do**
  if $\Gamma_i(t) = 1$ **then**
    for $j = 1 \to N$, $j \neq i$ & $\Phi_i(t) = 0$ **do**
      if $p^l_{j,l}(t) > 0$ & $\Gamma_j(t) = 1$ **then**
        set $\Lambda_i(t) = 0$.
        if $\Delta_j(t) = 0$ **then**
          set $\Delta_j(t) = 1$, $\Phi_i(t) = 1$, $\Upsilon_i(t) = 1$.
          $v_{i,lm}(t) = v_l + v^j_{i,lm}(t)$.
    if $\Lambda_i = 1$ **then**
      set $\Upsilon_i(t) = 1$.
      set $v_{i,lm}(t) = v_l$.
return result

January 5, 2023 2:17:51pm WSPC/284-US 2350002 ISSN: 2301-3850 2nd Reading

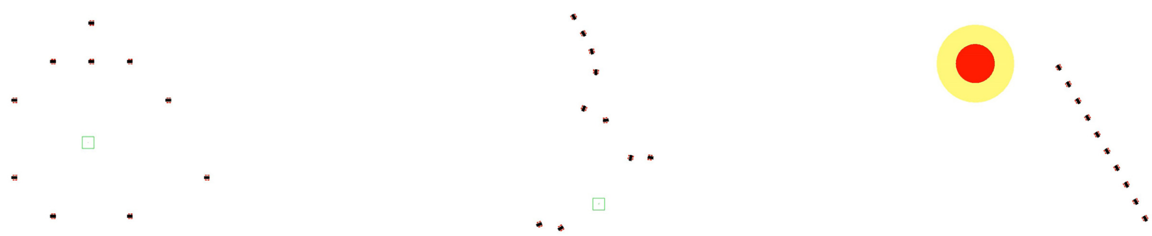

Phase 1

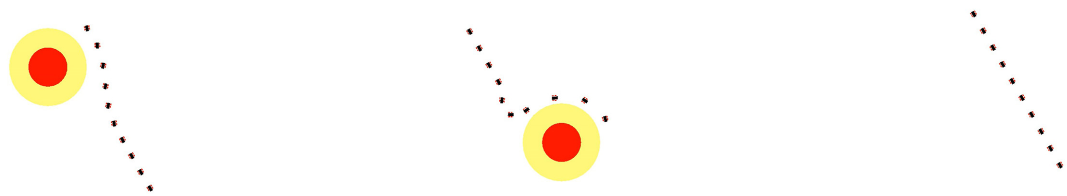

Phase 2

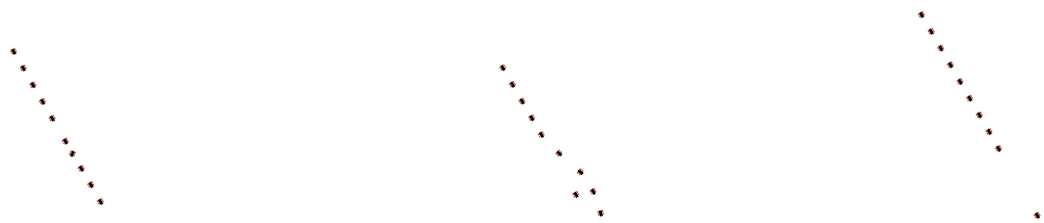

Phase 3

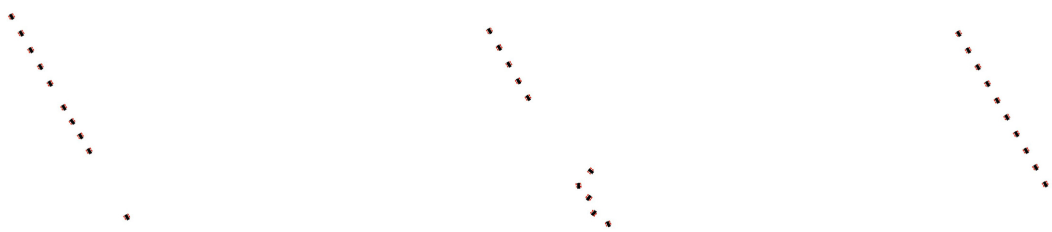

Phase 4

Fig. 9. Simulation results for robots modeled by unicycle models on ROS platform.

Different from the cases studied in Secs. 4 and 5, in ROS simulation, the linear and angular velocities of the robots are subject to saturation. For $i \in \underline{N}$, suppose $|\upsilon_i(t)| \leq \upsilon_{\max}$, $|\varpi_i(t)| \leq \omega_{\max}$.

Similar to the cases studied in Secs. 4 and 5, we consider a swarm of 10 robots. Let $T = 0.02$ s. The marching line are characterized by $v_l = (-0.25, 0.433)^T$, $\rho = 2$. For simplicity, the minimal inter-robot safety distance is set to be $\delta_i \triangleq \delta = 0.35$. Suppose $\upsilon_{\max} = 1$ m/s, $\omega_{\max} = 2$ rad/s. The control parameters are selected to be $\kappa_1 = 2.5$, $\kappa_2 = 10$, $a_i = 10$, $\omega_i = 0.3$, $\alpha = 1$, $\beta = 0.5$, $d_i = 0.2$. Note that $\kappa = 2/0.7 > 2.5 = \kappa_1$. Suppose there is a mobile obstacle with $\nu_1 = 2$ and $u_1(t) = (0.2133, 0.211)^T$.

The initial positions of the robots are given by $p_1(0) = (-4, 8)^T$, $p_2(0) = (0, 12)^T$, $p_3(0) = (-8, 4)^T$, $p_4(0) = (4, 8)^T$, $p_5(0) = (8, 4)^T$, $p_6(0) = (0, 8)^T$, $p_7(0) = (4, -8)^T$, $p_8(0) = (12, -4)^T$, $p_9(0) = (-4, -8)^T$, $p_{10}(0) = (-8, -4)^T$. The initial heading angles are given by $\vartheta_i(0) = 0$. The initial position for the obstacle is given by $q_1(0) = (-30, 23)^T$.

Similar to the case studied in Sec. 5, the whole simulation process consists of four phases:

(1) $t \in [0, 54]$s, the robots will asymptotically form a line from the initial position;
(2) $t \in [54, 130]$s, the robots will bypass the mobile obstacle and re-form a marching line;
(3) $t \in [130, 160]$s, robot 6 fails;
(4) $t \in [160, 218]$s robot 6 gets back to normal and rejoins the robot swarm.

Figure 9 shows the positions of the robot swarm and the obstacle during each phase, respectively. Similar to the

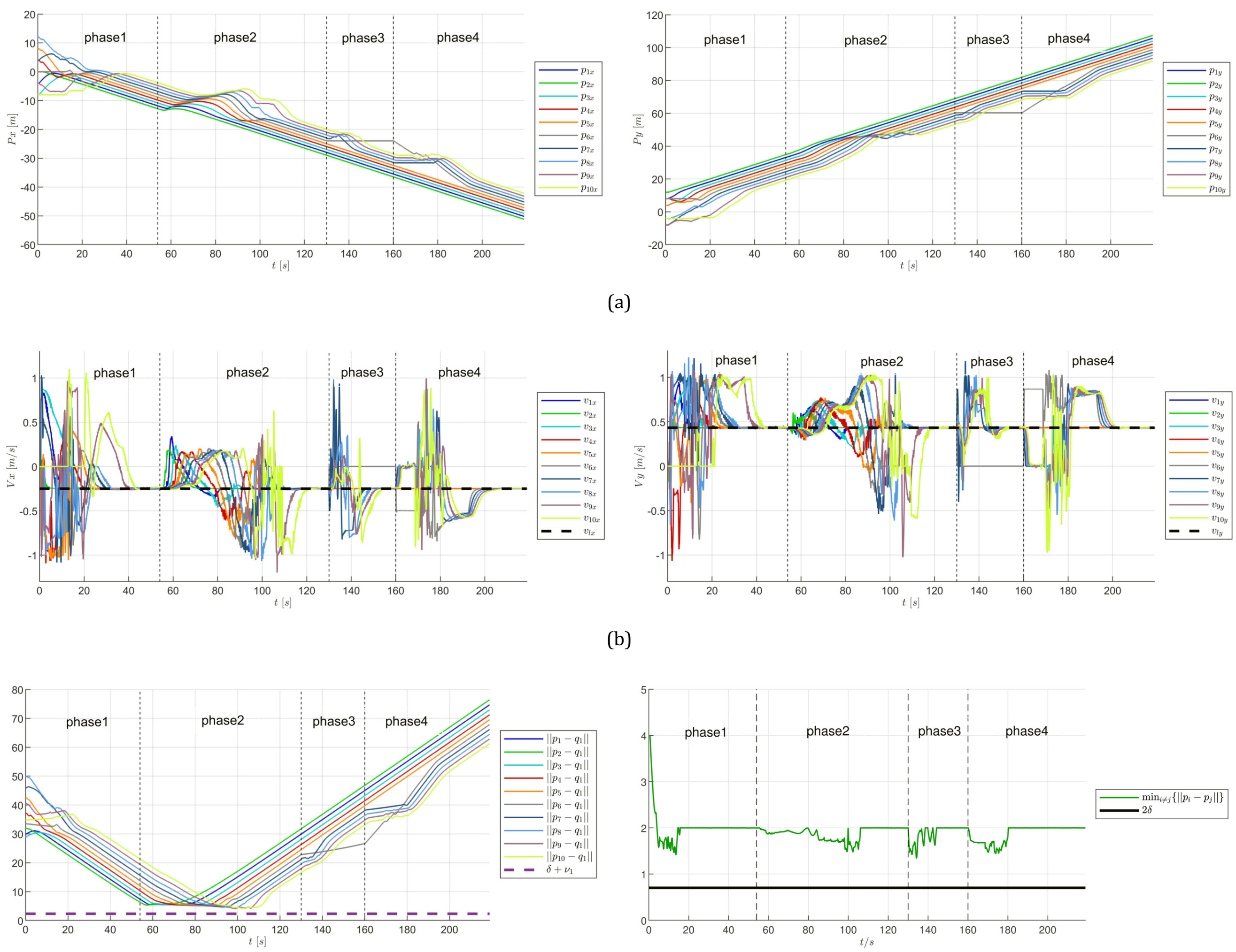

(a)

(b)

(c)

Fig. 10. Simulation result for robots modeled by unicycle models on ROS platform: (a) robots' positions; (b) robots' velocities; (c) relative distance between each robot and the mobile obstacle, and the minimal relative distance between two robots.

simulation results in Sec. 5, it can be observed that both the line marching objective and the collision avoidance objective have been achieved. Moreover, the algorithm proves to be robust against robot failure. Figures 10(a) and 10(b) show the time profiles of robots' positions and velocities, respectively. Figure 10(c) shows the relative distance between each robot and the mobile obstacle, and the minimal relative distance between two robots. These simulation results further confirm the effectiveness of the proposed algorithm.

7. Conclusion

This paper proposed a dynamic leader–follower approach to solving the line marching problem for a swarm of planar kinematic robots. In contrast to the existing exact formation algorithms, such as the virtual structure approach and the classic leader–follower approach, the proposed approach shows strong robustness against robot failure by constantly updating the leader–follower chain. Comprehensive numerical results considering different mathematical models are provided to validate the effectiveness of the proposed control algorithm.

Acknowledgments

This work was supported in part by National Natural Science Foundation of China under Grant Nos. 61703167, 62173149, and in part by Guangdong Nature Science Foundation under Grant No. 2021A1515012584.

References

[1] M. Dorigo, M. Birattari and T. Stutzle, Ant colony optimization, *IEEE Comput. Intell. Mag.* **1**(4) (2006) 28–39.

[2] C. M. Bishop *et al.*, The roller coaster flight strategy of bar-headed geese conserves energy during Himalayan migrations, *Science* **347** (6219) (2015) 250–254.

[3] X. Li, D. Zhu and Y. Qian, A survey on formation control algorithms for multi-AUV system, *Unmanned Syst.* **2**(4) (2014) 351–359.

[4] K. Oh, M. Park and H. Ahn, A survey of multi-agent formation control, *Automatica* **53** (2015) 424–440.

[5] X. Dong*Formation and Containment Control for High-order Linear Swarm Systems* (Springer-Verlag, Berlin, 2016).

[6] H. Liu and B. Zhu, *Formation Control of Multiple Autonomous Vehicle Systems* (John Wiley & Sons, 2018).

[7] H. Ahn*Formation Control: Approaches for Distributed Agents* (Springer Nature, Switzerland AG, 2020).

[8] M. A. Lewis and K.-H. Tan, High precision formation control of mobile robots using virtual structures, *Auton. Robots* **4**(4) (1997) 387–403.

[9] M. Egerstedt and M. Hu, Formation constrained multi-agent control, *IEEE Trans. Robot. Autom.* **17**(6) (2001) 947–951.

[10] K. D. Do and J. Pan, Nonlinear formation control of unicycle-type mobile robots, *Robot. Auton. Syst.* **55**(3) (2007) 191–204.

[11] Y. Liu and Y. Jia, An iterative learning approach to formation control of multi-agent systems, *Syst. Control Lett.* **61**(1) (2012) 148–154.

[12] X. Yu, X. Xu, L. Liu and G. Feng, Circular formation of networked dynamic unicycles by a distributed dynamic control law, *Automatica* **89** (2018) 1–7.

[13] X. Dong and G. Hu, Time-varying formation control for general linear multi-agent systems with switching directed topologies, *Automatica* **73** (2016) 47–55.

[14] W. Xiao, J. Yu, R. Wang, X. Dong, Q. Li and Z. Ren, Time-varying formation control for time-delayed multi-agent systems with general linear dynamics and switching topologies, *Unmanned Syst.* **7**(1) (2019) 3–13.

[15] X. Chai, J. Liu, Y. Yu, J. Xi and C. Sun, Practical fixed-time event-triggered time-varying formation tracking control for disturbed multi-agent systems with continuous communication free, *Unmanned Syst.* **9**(1) (2021) 23–34.

[16] Y. Zhang, Y. Wen, F. Li and Y. Chen, Distributed observer-based formation tracking control of multi-agent systems with multiple targets of unknown periodic inputs, *Unmanned Syst.* **7**(1) (2019) 15–23.

[17] J. P. Desai, J. P. Ostrowski and V. Kumar, Modeling and control of formations of nonholonomic mobile robots, *IEEE Trans. Robot. Autom.* **17**(6) (2001) 905–908.

[18] A. K. Das, R. Fierro, V. Kumar, J. P. Ostrowski, J. Spletzer and C. J. Taylor, A vision-based formation control framework, *IEEE Trans. Robot. Autom.* **18**(5) (2002) 813–825.

[19] G. Mariottini *et al.*, Vision-based localization for leader–follower formation control, *IEEE Trans. Robot.* **25**(6) (2009) 1431–1438.

[20] L. Consolini, F. Morbidi, D. Prattichizzo and M. Tosques, leader–follower formation control of nonholonomic mobile robots with input constraints, *Automatica* **44**(5) (2008) 1343–1349.

[21] J. Chen, D. Sun, J. Yang and H. Chen, A leader–follower formation control of multiple nonholonomic mobile robots incorporating receding-horizon scheme, *Int. J. Robot. Res.* **29**(6) (2010) 727–747.

[22] Y. Wang, M. Shan, Y. Yue and D. Wang, Vision-based flexible leader–follower formation tracking of multiple nonholonomic mobile robots in unknown obstacle environments, *IEEE Trans. Control Syst. Technol.* **28**(3) (2020) 1025–1033.

[23] L. Chen, J. Mei, C. Li and G. Ma, Distributed leader–follower affine formation maneuver control for high-order multiagent systems, *IEEE Trans. Autom. Control* **65**(11) (2020) 4941–4948.

[24] Z. Tang, R. Cunha, T. Hamel and C. Silvestre, Formation control of a leader–follower structure in three-dimensional space using bearing measurements, *Automatica* **128** (2021) 567–573.

[25] F. Chen and D. V. Dimarogonas, Leader–follower formation control with prescribed performance guarantees, *IEEE Trans. Control Netw. Syst.* **8**(1) (2021) 450–461.

[26] I. Buckley and M. Egerstedt, Infinitesimal shape-similarity for characterization and control of bearing-only multirobot formations, *IEEE Trans. Robot.* **37**(6) (2021) 1921–1935.

[27] W. Ren and E. Atkins, Distributed multi-vehicle coordinated control via local information exchange, *Int. J. Robust Nonlinear Control* **17**(10–11) 1002–1033.

January 5, 2023 2:18:47pm WSPC/284-US 2350002 ISSN: 2301-3850 2nd Reading

He Cai received his B. Eng. degree in automation from the University of Science and Technology of China, Hefei, China, in 2010, and Ph.D. degree in mechanical and automation engineering from the Chinese University of Hong Kong, Hong Kong, China, in 2014. From 2014 to 2017, he worked as a research fellow with the School of Electrical and Electronic Engineering, the Nanyang Technological University, Singapore. Since 2017, he has been a full professor with School of Automation Science and Engineering, the South China University of Technology, Guangzhou, China. His research interests involve cooperative control of multiagent systems and its applications in intelligent robots and smart grid.

Shuping Guo received his B. Eng. degree in automation from the Tianjin University of Technology, Tianjin, China, in 2019, and is currently pursuing the M. Eng. degree in control science and engineering at the South China University of Technology, Guangzhou, China. His current research interests focus on swarm system modeling and control.

Huanli Gao received his B. S. and M. S. degrees from Shandong University, Jinan, China, in 2002 and 2005, respectively, and the Ph.D. degree from South China University of Technology, Guangzhou, China, in 2008. From October 2007 to April 2008, she received national support to study at the School of Electrical and Electronic Engineering, Nanyang Technological University in Singapore. She is currently working in the School of Automation Science and Engineering, South China University of Technology. Her current research interests include autonomous vehicle control, cooperative control, networked control systems.